Supplementary Information

Ultra-stable and poison tolerant oxygen evolution activity enabled by surface $In_2O_{3-x}(OH)_y$ of $Co_3In_2S_2$ large single crystals

Anjaiah Sheelam,[a] Ariel Whitten,[b, =] Carrington Gates Moore,[b, =] Mark Engelhard,[c] Jean-Sabin McEwen,[a,b,d,e,f] and Jeffrey G. Bell[a,b] *

[a]Department of Chemistry, Washington State University, Pullman, Washington 99164, United States.

[b]The Gene and Linda Voiland School of Chemical Engineering and Bioengineering, Washington State University, Washington 99164, United States.

[c]Environmental Molecular Sciences Laboratory, Pacific Northwest National Laboratory, Innovation Blvd, Richland-99354, Washington, United States.

[d]Institute for Integrated Catalysis, Pacific Northwest National Laboratory, Innovation Blvd, Richland-99354, Washington, United States.

[e]Department of Physics and Astronomy, Washington State University, Washington 99164, United States.

[f]Department of Biological Systems Engineering, Washington State University, Washington 99164, United States.

Correspondence to Jeffrey.g.bell@wsu.edu

Materials: High-pure indium beads (In; 99.999%), cobalt powder (Co; 99.995 %), and sulfur (S; 99.998 %) powders were purchased from Sigma-Aldrich, United States of America (USA) and stored in argon atmosphere-controlled glove box. Iodine (I_2, 99.99%) and Silver conductive paste purchased from Sigma-Aldrich, USA. Silicon glue was obtained from the Gorilla Glue Company, USA. Fused quartz tubes of 1 cm inner diameter with 1 mm wall thickness were purchased from Technical Glass Products.inc, USA. Oxygen (99 %) and acetylene gas cylinder were purchased from university stores, at Washington State University, USA.

Schemes, Tables and Figures:

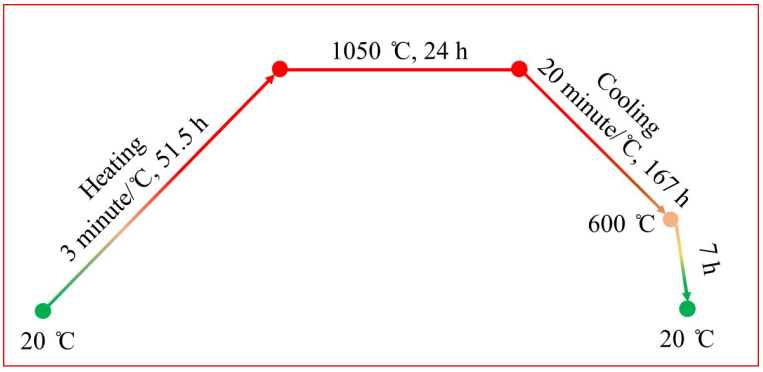

Scheme S1. Illustrates the temperature program for the synthesis of $Co_3In_2S_2$ single-crystals in a single-zone furnace.

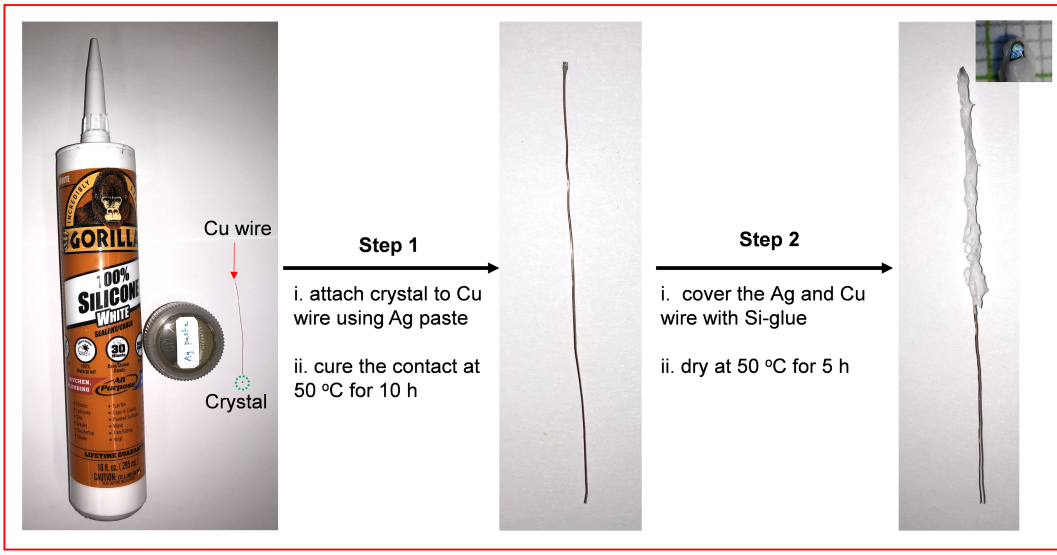

Scheme S2. Fabrication protocol of the electrode for electrochemical oxygen production.

Table S1. Lists the lattice parameters of $Co_3In_2S_2$ measured from SC-XRD, our DFT-based model and comparison with the literature.

$Co_3In_2S_2$	Lattice Parameters (a, b, c (Å); α, β, γ(°))	Space group	Cell volume (Å^3)
Measured	5.328, 5.328, 13.688; 90.0, 90.0, 120.0	$R\bar{3}m$	337.0
Refinement	5.311, 5.311, 13.650; 90.0, 90.0, 120.0	$R\bar{3}m$	333.5
DFT-based Model	5.322, 5.322, 13.621; 90.0, 90.0, 120.0	$R\bar{3}m$	334.1

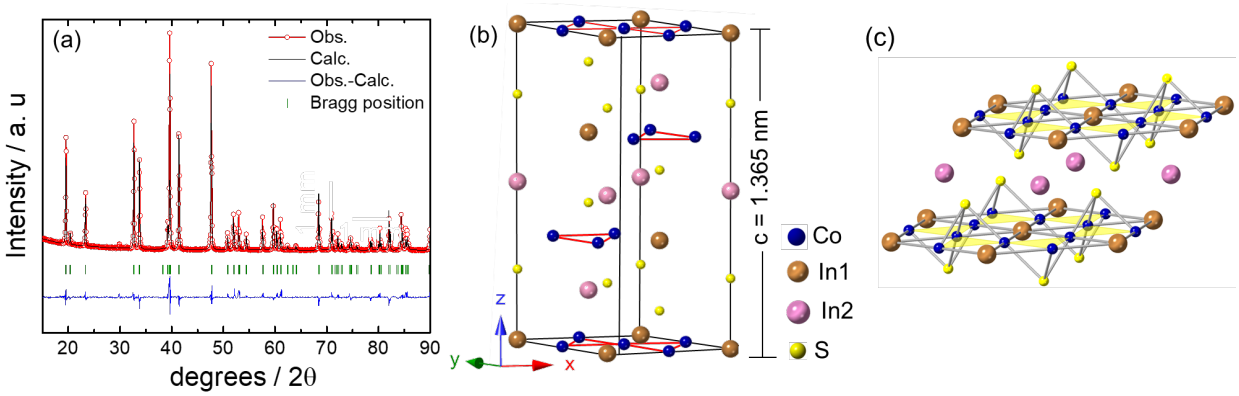

Fig. S1 Rietveld refinement of XRD pattern of $Co_3In_2S_2$ and (b) the crystal structure of $Co_3In_2S_2$ obtained from Rietveld refinement. (c) The Kagome lattice of $Co_3In_2S_2$ hosts two different In-sites.

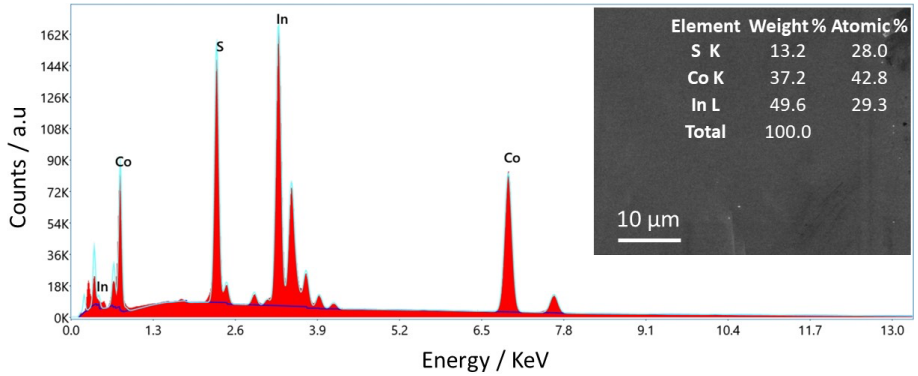

Fig. S2 (a) Energy dispersive X-ray analysis spectrum of single crystal $Co_3In_2S_2$ with weight and atomic percentages of elements.

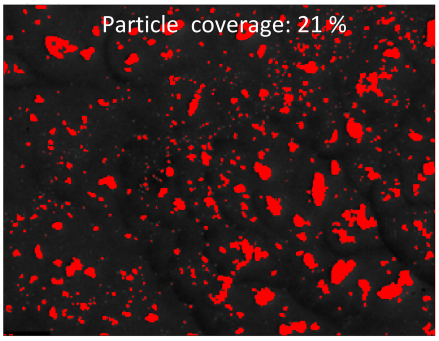

Fig. S3 The coverage of $Co_3In_2S_2$ powder particles on the GC electrode. (Calculated using ImageJ software)

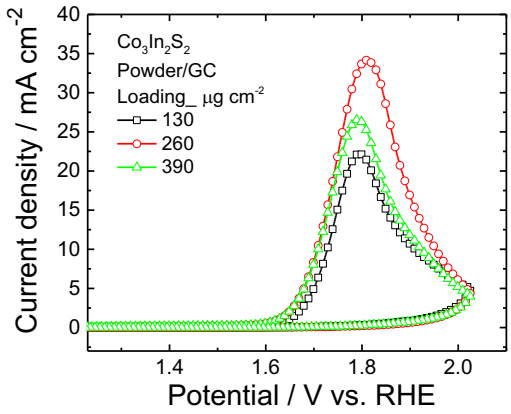

Fig. S4 Mass loading study of OER activity of Powder/GC in 1 M KOH.

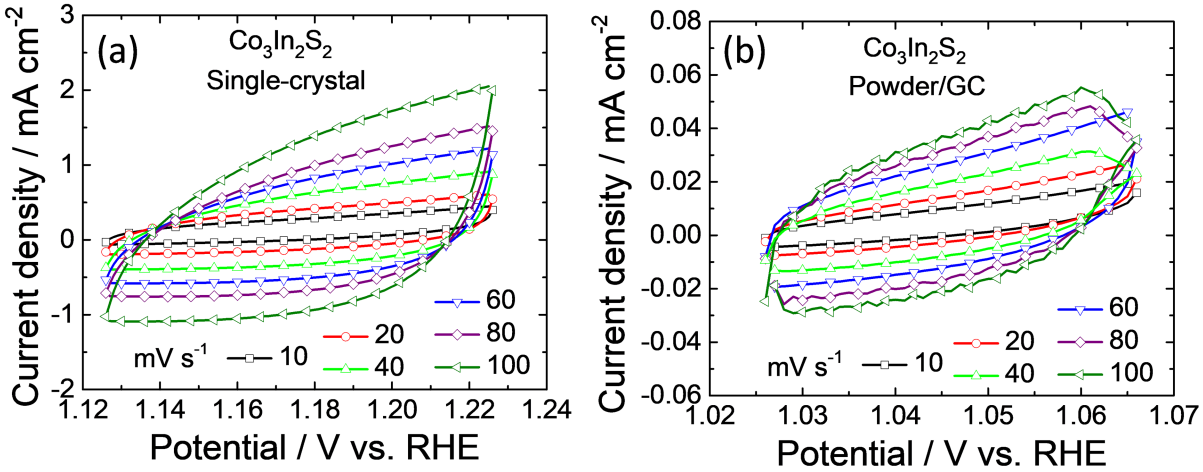

Fig. S5 Cyclic voltammograms of $Co_3In_2S_2$ and Powder/GC were acquired at different scanning rates from 10, 20, 40, 60, 80, and 100 mV s^{-1} in 1 M KOH.

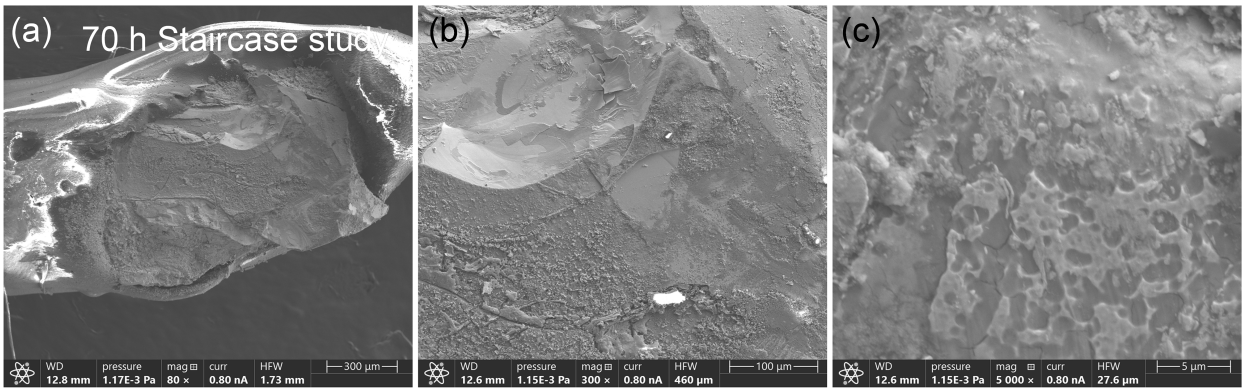

Fig. S6 (a)-(c) Morphology of the single-crystal $Co_3In_2S_2$ electrode after the 70 h of multicurrent process (10, 25, 50, 100, 200, 250 and 10 mA cm^{-2}) of OER.

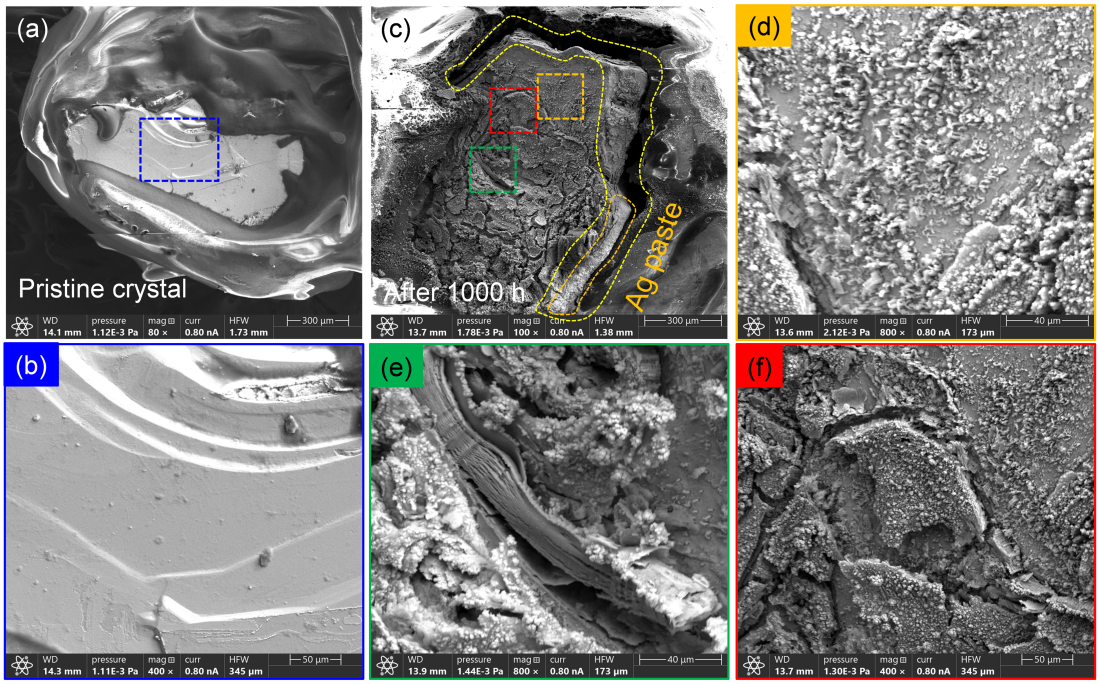

Fig. S7 (a)-(b) the surface of pristine single-crystal $Co_3In_2S_2$ electrode and (c)-(f) morphology of single-crystal $Co_3In_2S_2$ after 1000 h durability test.

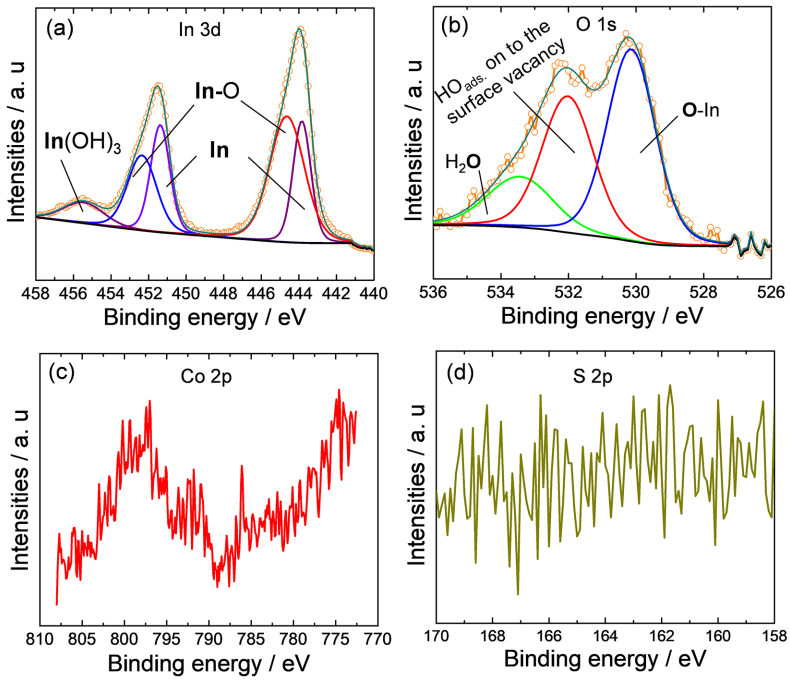

Fig. S8 High-resolution XPS spectra of (a) In 3*d*, (b) O 1*s*, (c) Co 2*p*, and (d) S 2*p* of single-crystal $Co_3In_2S_2$ after 1000 h durability test.

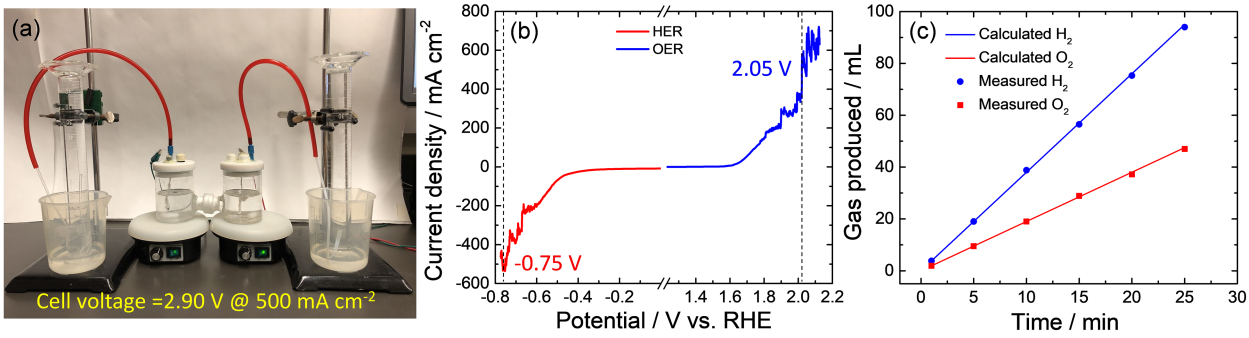

Fig. S9 (a) The H-cell configuration of WE assembled with single-crystal $Co_3In_2S_2$ electrodes as anode and cathode and (b) H_2 and O_2 evolution polarization curves (without *iR*-correction) of single-crystal $Co_3In_2S_2$ obtained from 3-electrode measurement. (c) Comparison of the H_2 and O_2 products generated by WE with theoretical values.

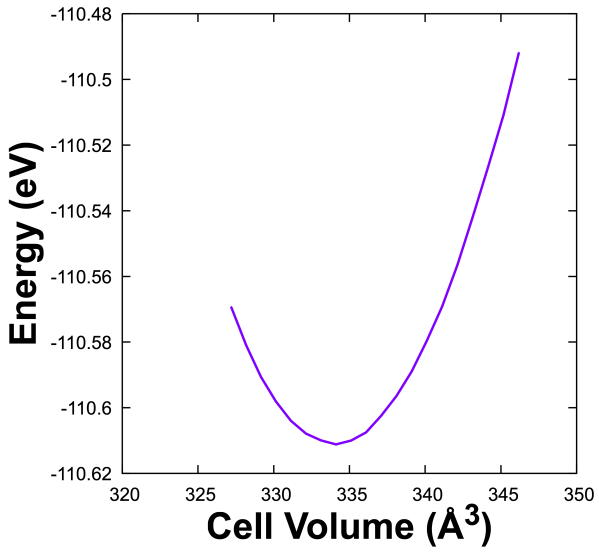

Fig. S10 Energy vs. volume curve for the optimization of the bulk unit cell. The bulk unit cell parameters are given in Table S1.

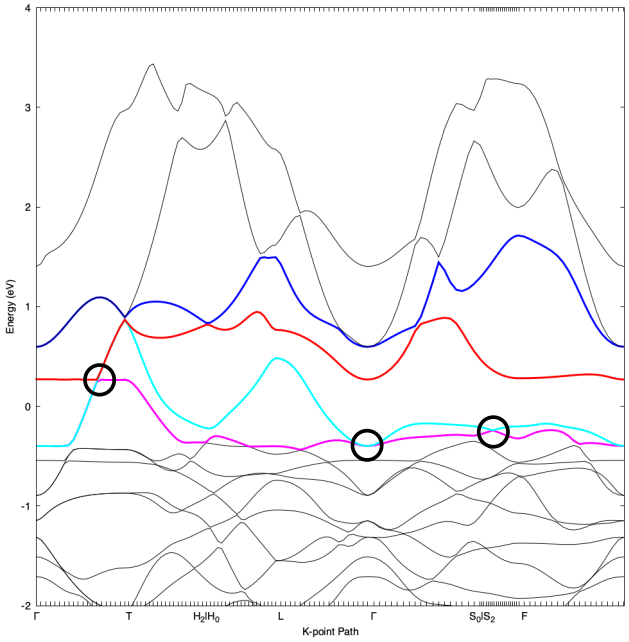

Fig. S11 The band structure of the bulk $Co_3In_2S_2$ intersecting bands are highlighted in different colors; circles highlight points of crossing. (The band crossings between the Γ and F-points are identified as Wely points.)

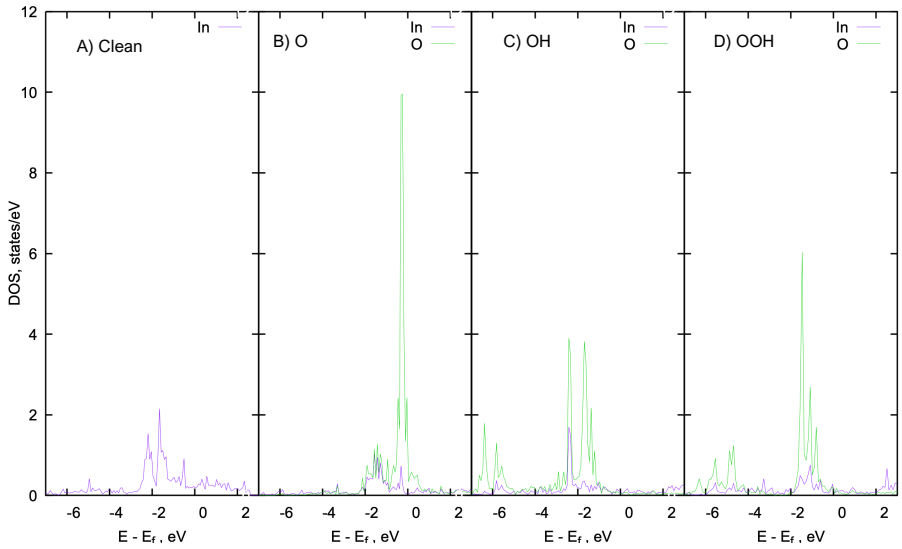

Fig. S12 PDOS for the p-orbital of selected Indium and respective adsorbed oxygen atoms in the above cases B-D; A is referencing a clean surface with no adsorbates.

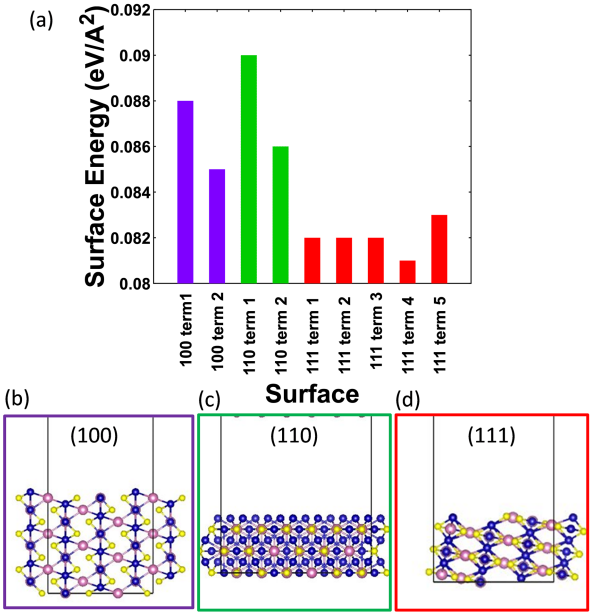

Fig. S13 (a) Comparison of surface energies of different terminations for each facet. (b)-(d) the most favorable termination for (100), (110) and (111) facets, respectively.

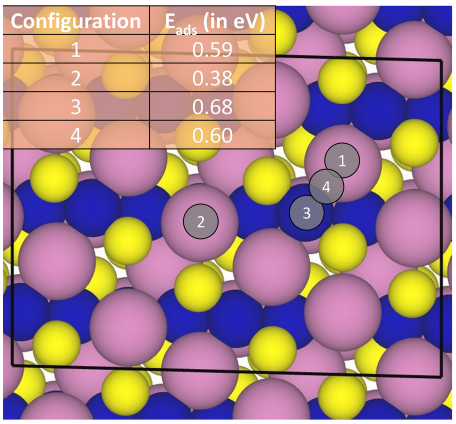

Fig. S14 Adsorption energies of OOH^- intermediate calculated at four possible sites (1. In1-site, 2. In2-site, 3. Co-site and 4. Co-In1).

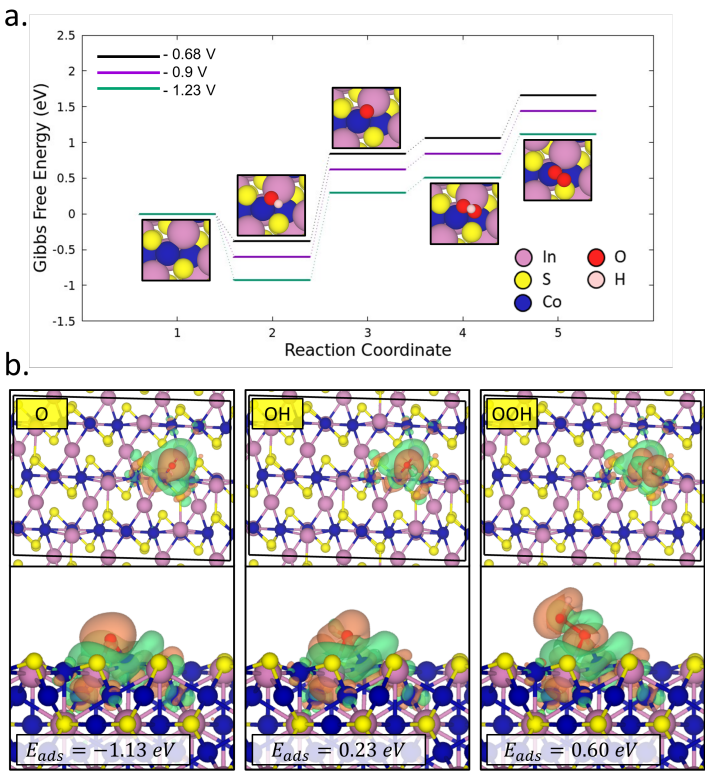

Fig. S15 (a) The OER mechanism on the Co-In1 bridge site by reaction coordinate *vs*. Gibbs Free Energy at T=293 K. The effects of a potential are shown by different line colors with values in the key. (b) Charge transfer calculations for the reaction intermediates for the OER on the Co-In1 the surface gaining charge. The red areas indicate a charge loss while the green areas indicate a charge gain. The isosurface used is 0.005 electrons/$Bohr^3$.